Article

Root-Growth Mechanism for Single-Walled Boron Nitride Nanotubes in Laser Vaporization Technique

Raul Arenal, Odile Stephan, Jean-Lou Cochon, and Annick Loiseau

J. Am. Chem. Soc., **2007**, 129 (51), 16183-16189 • DOI: 10.1021/ja076135n

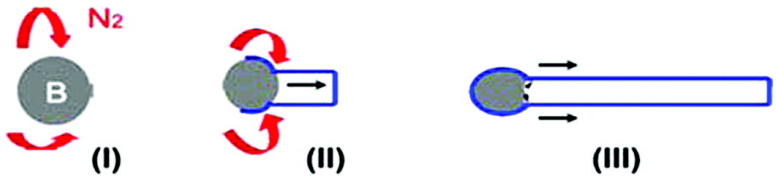

More About This Article

Additional resources and features associated with this article are available within the HTML version:

- Supporting Information
- Links to the 6 articles that cite this article, as of the time of this article download
- Access to high resolution figures
- Links to articles and content related to this article
- Copyright permission to reproduce figures and/or text from this article

View the Full Text HTML

J|A|C|S
ARTICLES
Published on Web 12/05/2007

Root-Growth Mechanism for Single-Walled Boron Nitride Nanotubes in Laser Vaporization Technique

Raul Arenal,*[,†,‡] Odile Stephan,[§] Jean-Lou Cochon,[||] and Annick Loiseau[†]

Laboratoire d'Etude des Microstructures, ONERA-CNRS (UMR 104), 92322 Châtillon, France, Materials Science Division, Argonne National Laboratory, Illinois 60439, Laboratoire de Physique des Solides, UMR CNRS 8502, Université Paris-Sud, 91405 Orsay, France, and Département Matériaux et Systèmes Composites, ONERA, 91761 Palaiseau, France

Received August 28, 2007; E-mail: raul.arenal@onera.fr

Abstract: We present a detailed study of the growth mechanism of single-walled boron nitride nanotubes synthesized by laser vaporization, which is the unique route known to the synthesis of this kind of tube in high quantities. We have performed a nanometric chemical and structural characterization by transmission electron microscopy (high-resolution mode (HRTEM) and electron energy loss spectroscopy) of the synthesis products. Different boron-based compounds and other impurities were identified in the raw synthesis products. The results obtained by the TEM analysis and from the synthesis parameters (temperature, boron, and nitrogen sources) combined with phase diagram analysis to provide identification of the fundamental factors determining the nanotube growth mechanism. Our experiments strongly support a root-growth model that involves the presence of a droplet of boron. This phenomenological model considers the solubility, solidification, and segregation phenomena of the elements present in this boron droplet. In this model, we distinguish three different steps as a function of the temperature: (1) formation of the liquid boron droplet from the decomposition of different boron compounds existing in the hexagonal boron nitride target, (2) reaction of these boron droplets with nitrogen gas present in the vaporization chamber and recombination of these elements to form boron nitride, and (3) incorporation of the nitrogen atoms at the root of the boron particle at active reacting sites that achieves the growth of the tube.

1. Introduction

Nanostructured materials have attracted ever increasing attention over the past several years due to their unique properties and many specific potential applications. Among these materials, nanotubes play a special role. Carbon nanotubes (CNTs), which were first discovered in 1991,[1] are the most commonly studied nanotubes and are investigated in various domains such as molecular electronics and optoelectronics.[2] A few years later, boron nitride nanotubes (BNNTs) follow the same trend. On the basis of structural similarities between graphite and hexagonal boron nitride (h-BN), their stability has been theoretically predicted in 1994,[3−5] and shortly after, the synthesis of both multi-walled (MW−BNNT) and single-walled (SW−BNNT) tubes has been realized, in 1995[6] and 1996,[7] respectively. In contrast to CNTs, BNNTs are insulators with a band gap close to 6 eV, independent of the number of layers in the tube and the tube diameter and helicity.[5,8−10] As a consequence, these tubes may be used for high-power-high-frequency electronic devices and for optoelectronic applications.[11] BNNTs possess outstanding mechanical properties in common with their carbon counterpart. The elastic Young modulus of BNNTs has been determinated to be over 1 TPa.[12] Furthermore, these BN tubes are chemically inert and can operate as protective cages at the nanoscale.[13] Among other properties, the combination of metal/semiconducting C− and insulating BN− tubes give rise to a large variety of one-dimensional heterojunctions (band-offset engineering),[14,15] coaxial nanocables,[16] and field emission.[17,18]

[†] Laboratoire d'Etude des Microstructures.
[‡] Argonne National Laboratory.
[§] Laboratoire de Physique des Solides.
[||] ONERA.

(1) Iijima, S. *Nature* **1991**, *354*, 56.
(2) Dresselhaus, M. S., Dresselhaus, G., Avouris, Ph., Eds. *Carbon nanotubes: synthesis, structure, properties, and applications*; Springer-Verlag: Berlin, 2001.
(3) Blase, X.; Rubio, A.; Louie, S. G.; Cohen, M. L. *Europhys. Lett.* **1994**, *28*, 335.
(4) Rubio, A.; Corkill, J. L.; Cohen, M. L. *Phys. Rev. B* **1994**, *49*, 5081.
(5) Blase, X.; Rubio, A.; Louie, S. G.; Cohen, M. L. *Phys. Rev. B* **1995**, *51*, 6868.
(6) Chopra, N. G.; Luyken, R. J.; Cherrey, K.; Crespi, V. H.; Cohen, M. L.; Louie, S. G. *Science* **1995**, *269*, 966.
(7) Loiseau, A.; Willaime, F.; Demoncy, N.; Hug, G.; Pascard, H. *Phys. Rev. Lett.* **1996**, *76*, 4737.
(8) Arenal, R.; Stephan, O.; Kociak, M.; Taverna, D.; Loiseau, A.; Colliex, C. *Phys. Rev. Lett.* **2005**, *95*, 127601.
(9) Arenal, R.; Stephan, O.; Kociak, M.; Taverna, D.; Loiseau, A.; Colliex, C. *Microsc.d Microanal.* **2006**, *12*, 1166.
(10) Arenal, R.; Stephan, O.; Kociak, M.; Taverna, D.; Loiseau, A.; Colliex, C. *Microsc. Microanal.* **2007**.
(11) Radosavljevic, M.; Appenzeller, J.; Derycke, V.; Martel, R.; Avouris, P.; Loiseau, A.; Cochon, J.-L.; Pigache, D. *Appl. Phys. Lett.* **2003**, *82*, 4131.
(12) Chopra, N. G.; Zettl, A. *Solid State Comm.* **1998**, *105*, 297.
(13) Han, W.; Redlich, P.; Ernst, F.; Ruhle, M. *Appl. Phys. Lett.* **1999**, *75*, 1875.
(14) Blase, X.; Charlier, J. C.; DeVita, A.; Car, R. *Appl. Phys. Lett.* **1997**, *70*, 197.
(15) Meunier, V.; Roland, C.; Bernholc, J.; Buongiorno-Nardelli, M. *Appl. Phys. Lett.* **2002**, *81*, 46.
(16) Zhang, Y.; Suenaga, K.; Colliex, C.; Iijima, S. *Science* **1998**, *281*, 973.
(17) Dorozhkin, P.; Golberg, D.; Bando, Y.; Dong, Z. C. *Appl. Phys. Lett.* **2002**, *81*, 1083.

10.1021/ja076135n CCC: $37.00

Following the pioneering synthesis works, several teams have produced these tubes employing different methods of synthesis at low/medium temperature (300−2000 °C, e.g., refs 19−21 and 23−25) or at high-temperature ranges (over 2000 °C, e.g., refs 7 and 26−31). A survey of these works should allow growth parameters such as temperature, sources of B and N, and in some cases, choice of catalytic particle, to be correlated with tube characteristics like diameter, length, and crystallinity. As these relations are critical to an as of yet unattained understanding of the formation process of BNNTs, we review the previous experiments in detail below.

Boron oxide is the most frequently used source of boron in the synthesis of BNNTs. It is used in various CVD techniques[32,33] involving the vapor−liquid−solid (V−L−S) mechanism[24,34] and for all processes that employ the carbothermic method.[13,19,20,35] There are three other main sources of boron: (1) Solid hexagonal or cubic BN is used as a target and decomposed in synthesis techniques employing laser ablation/vaporization[26,27,29−31] and also an arc discharge.[6,36] (2) Metal diborides (metal is hafnium, zirconium, or lanthanum)[7,28] and mixtures of boron and borides are also often decomposed when using an arc discharge to synthesize BNNTs.[37] (3) Finally, powders of boron, h-BN, or borides are used in the ball milling process.[21,22]

Sources of nitrogen are far less varied. In most cases, it is injected directly as an elemental gas or as ammonia, except when it is required in specific compounds of nitrogen to facilitate synthesis via chemical reaction[23,38,40] or is available from the decomposition of the boron nitride.[6,41]

The temperature of synthesis is dictated by the source of boron and the synthesis method. Four distinct regimes may be distinguished. These are: (1) above 2400 °C if the boron source is solid BN, a boride, or pure boron material as for the laser-ablation and arc discharge techniques; (2) between 1300 and 1700 °C when using boron oxide in a gaseous form for most CVD techniques; (3) close to 1300 °C for synthesis involving the V−L−S mechanism or "ball milling"; and (4) between 400 and 1100 °C if using volatile boron precursors, e.g., in some CVD processes.[23,38,40,42]

Considering those synthesis involving catalytic particles, the choice is generally the same as for the synthesis of CNTs, namely, iron, cobalt, nickel, or aluminum,[21,22,28,39,40,42,43] although the necessity of using these catalysts has not yet been justified.

Turning to the effect of the synthesis technique and exact parameters on the morphology of the BNNTs, it is remarkable that no strong correlations emerge from the survey of experiments. In fact, despite the large variations in experimental conditions and the large range of synthesis techniques, BNNTs present a large heterogeneity of diameters, lengths, and shapes, even in a single synthesis experiment. Most of the techniques are restricted to the synthesis of MWNTs, which are not as suitable as SWNTs for studying and modeling the intrinsic properties of this kind of tubes. This situation changed in 2001 due to the laser vaporization technique developed at ONERA. Using this technique, we have succeeded in producing SW-BNNTs in a high quantity and with a high crystalline quality,[30,44] opening the way toward the study of their properties.[8−11,45,46] This technique is so far the unique route to the synthesis of single-walled BNNTs in high quantities. Also, the relative structural homogeneity of BNNTs thus produced by this way provides the first real opportunity to speculate about the growth mechanism.

In contrast to SW-CNTs, where the growth mechanism has been studied by several groups (e.g., refs 47 and 48), relatively little is known about the formation of BNNTs. For instance, for SW-CNTs, the influence of the metal catalysts in the growth of the tubes is well established and their role becomes clear.[48] The catalyst has been shown to have the ability to dissolve the carbon and to reject it upon solidification, permitting the graphitization at very low temperatures. Nevertheless, in the case of BNNTs, both aspects, influence and role of the catalysts, are still missing and they have not yet been demonstrated. We note that the only work developed in this way for BNNTs is this one of Velazquez et al.[42] These authors produce multi-walled bamboo-like BNNTs (diameter of several nanometers) using a ball-milling synthesis method and propose a root-growth mechanism of the tubes that involves the Fe−Ni−Cr catalytic particles. Indeed, in our approach, SW-BNNTs are produced

(18) Cumings, J.; Zettl, A. In *Electronic Properties of Molecular Nanostructures*; Kuzmany, H., et al., Eds.; AIP: Melville, NY, 2001; p 577.
(19) Han, W.; Bando, Y.; Kurashima, K.; Sato, T. *Appl. Phys. Lett.* **1998**, *73*, 3085.
(20) Golberg, D.; Bando, Y.; Han, W.; Kurashima, K.; Sato, T. *Chem. Phys. Lett.* **1999**, *308*, 337.
(21) Chen, Y.; Gerald, J. F.; Williams, J. S.; Bulcock, S. *Chem. Phys. Lett.* **1999**, *299*, 260.
(22) Chen, Y.; Chadderton, L. T.; Gerald, J. F.; Gerald, J. F.; Williams, J. S. *Appl. Phys. Lett.* **1999**, *74*, 2960.
(23) Shelimov, K. B.; Moskovits, M. *Chem. Mater.* **2000**, *12*, 250.
(24) Tang, C. C.; Lamy de la Chapelle, M.; Li, P.; Liu, Y. M.; Dang, H. Y.; Fan, S. S. *Chem. Phys. Lett.* **2001**, *342*, 492.
(25) Terauchi, M.; Tanaka, M.; Matsuda, H.; Takeda, M.; Kimura, K. *J. Electron Microsc.* **1997**, *1*, 75.
(26) Golberg, D.; Bando, Y.; Eremets, M.; Takemura, K.; Kurashima, K.; Yusa, H. *Appl. Phys. Lett.* **1996**, *69*, 2045.
(27) Yu, D. P.; Sun, X. S.; Lee, C. S.; Bello, I.; Lee, S. T.; Gu, H. D.; Leung, K. M.; Zhou, G. W.; Dong, Z. F.; Zhang, Z. *Appl. Phys. Lett.* **1998**, *72*, 1966.
(28) Cumings, J.; Zettl, A. *Chem. Phys. Lett.* **2000**, *316*, 211.
(29) Laude, T.; Matsui, Y.; Marraud, A.; Jouffrey, B. *Appl. Phys. Lett.* **2000**, *76*, 3239.
(30) Lee, R. S.; Gavillet, J.; Lamy de la Chapelle, M.; Loiseau, A.; Cochon, J.-L.; Pigache, D.; Thibault, J.; Willaime, F. *Phys. Rev. B* **2001**, *64*, 121405-(R).
(31) Golberg, D.; Rode, A.; Bando, Y.; Mitome, M.; Gamaly, E.; Luther-Davies, B. *Diamond Relat. Mater.* **2003**, *12*, 1269.
(32) Ma, R.; Bando, Y.; Sato, T. *Chem. Phys. Lett.* **2001**, *337*, 61.
(33) Tang, C. C.; Bando, Y.; Sato, T.; Kurashima, K. *Chem. Commun.* **2002**, *12*, 1290.
(34) Bae, S. Y.; Seo, H. W.; Park, J.; Choi, Y. S.; Park, J. C.; Lee, S. Y. *Chem. Phys. Lett.* **2003**, *374*, 534.
(35) Deepak, F. L.; Vinod, C. P.; Mukhopadhyay, K.; Govindaraj, A.; Rao, C. N. R. *Chem. Phys. Lett.* **2002**, *353*, 345.
(36) Terrones, M.; Srivastava, D.; Terrones, H.; Zhang, J. P.; Ramos, S.; Hare, J. P.; Castillo, R.; Prasides, K.; Cheethan, A. K.; Kroto, H. W.; Walton, D. R. M. *Chem. Phys. Lett.* **1996**, *259*, 568.
(37) Kuno, M.; Oku, T.; Suganuma, K. *Diamond Relat. Mater.* **2001**, *10*, 1231.
(38) Lourie, O. R.; Jones, C. R.; Bartlett, B. M.; Gibbons, P. C.; Ruoff, R. S.; Buhro, W. E. *Chem. Mater.* **2000**, *12*, 1808.
(39) Fitz Gerald, J. D.; Chen, Y.; Conway, M. J. *Appl. Phys. A.* **2003**, *76*, 07.
(40) Chen, X.; Wang, X.; Liu, J.; Wang, Z.; Qian, Y. *Appl. Phys. A* **2004**, *81*, 1035.
(41) Shimizu, Y.; Moriyoshi, Y.; Komatsu, S.; Ikegami, T.; Ishigaki, T.; Sato, T.; Bando, Y. *Thin Solid Films* **1998**, *316*, 178.
(42) Velazquez-Salazar, J. J.; Muñoz-Sandoval, E.; Romo-Herrera, J. M.; Lupo, F.; Rüle, M.; Terrones, H.; Terrones, M. *Chem. Phys. Lett.* **2005**, *416*, 342.
(43) Ma, R.; Bando, Y.; Sato, T.; Kurashima, K. *Chem. Mater.* **2001**, *13*, 2965.
(44) Arenal, R. Ph.D. Thesis, Universite Paris XI - Orsay, 2005.
(45) Arenal, R.; Ferrari, A. C.; Reich, S.; Wirtz, L.; Mevellec, J.-Y.; Lefrant, S.; Rubio, A.; Loiseau, A. *Nano Letters* **2006**, *6*, 1812.
(46) Lauret, J. S.; Arenal, R.; Ducastelle, F.; Loiseau, A.; Cau, M.; Attal-Tretout, B.; Rosencher, E.; Goux-Capes, L. *Phys. Rev. Lett.* **2005**, *94*, 037405.
(47) Saito, Y.; Yoshikawa, T.; Okuda, M.; Fujimoto, N.; Yamamuro, S.; Wakoh, K.; Sumiyama, K.; Suzuki, K.; Kasuya, A.; Nishina, Y. *Jpn. J. Appl. Phys.* **1994**, *33*, 526; Saito, Y.; Yoshikawa, T.; Okuda, M.; Fujimoto, N.; Yamamuro, S.; Wakoh, K.; Sumiyama, K.; Suzuki, K.; Kasuya, A.; Nishina, Y. *Carbon* **1995**, *33*, 979.
(48) Gavillet, J.; Loiseau, A.; Journet, C.; Willaime, F.; Ducastelle, F.; Charlier, J.-C. *Phys. Rev. Lett.* **2001**, *87*, 275504.

without a catalyst; nanotube growth proceeds from a pure boron nanoparticle[30] following the mechanism that we present in this paper.

In this work, we report a systematic and detailed transmission electron microscopy study (HRTEM and EELS) performed on SW-BNNTs and byproducts obtained during the laser vaporization process. This TEM study combined with the analysis of the synthesis conditions and the thermodynamic data from the literature provides important clues on the formation mechanism of BNNTs. We will show that all these data strongly support a root-growth mechanism, with boron nanoparticles acting as growth precursors.

2. Experimental Section

Our setup of synthesis of SW-BNNTs is based on the continuous heating of a h-BN target by a CO_2 (wavelength 10.6 μm) continuous laser under a partial pressure of nitrogen gas. The reaction chamber is vertically oriented, and a nitrogen flow is introduced at its bottom in such a way as to carry out the vaporized material up to the top of the chamber. The temperature at the surface of the target is measured by an optical pyrometer (silicon photodiode) and is equal to 3200−3500 K. The temperature of the nitrogen gas has been measured by coherent anti-Stokes Raman scattering (CARS) as a function of the distance to the target surface.[50,51] These measurements indicate that, in the vicinity of the target surface, the nitrogen gas is heated up to its temperature and plays the role of a local furnace. Above the target, its temperature decreases first rapidly (cooling rate is about 300 K/ms within a layer of 3 mm thick above the target surface that is between 3500 and 2200 K) and then more slowly in such a way as to reach a plateau (temperature is around 1200 K) at a distance of 7 mm above the target surface. The target is a commercial (Carborundum/Saint-Gobain, Inc.) h-BN cylinder that rotates and translates vertically at constant speed during the synthesis process to ensure uniform vaporization. It is made of h-BN powder pressed with boron oxide (B_2O_3) as binding material. The exact composition (in wt %) of the target is: 91.2% BN, 4.0% O, 4.5% B_2O_3, 0.1% Ca, 0.02% C, and 0.18% other impurities.

We optimized the synthesis parameters (nitrogen pressure in the vaporization chamber, nitrogen flow, and temperature at the surface of the target/laser power) to improve the quantity and quality of the tubes.[44,52] Indeed, we established that the optimized conditions occur for the follow couple pressure-gas flow: 1000 mbar - 100 mL/s, 1200 mbar - 120 mL/s, and 800 mbar - 80 mL/s. These couple pressure-flow conditions correspond to identical velocity of gas at the entry of the vaporization chamber. We also optimized the laser power and this value must be between 1000 and 1200 W. This power is equivalent to a temperature at the surface of the target above 2400 °C. Working under these conditions, we usually obtain between 500 and 550 mg/h of raw products that contain a high quantity of nanotubes.

The as-synthesized product was ultrasonicated in ethanol and the solution was dispersed onto copper grids coated with an amorphous carbon film with holes in order to carry out transmission electron microscopy (TEM) and electron energy loss spectroscopy (EELS) studies. Structural TEM work was performed with Philips CM-20 and Jeol 4000-EX microscopes, operating at 200 and 400 kV, respectively, and chemical analyses were done with spatially resolved EELS using a dedicated scanning transmission electron microscope (STEM) VG HB 501 working at 100 kV. The cold field emission gun of the STEM is a very high brightness source. This allows the formation of small probes (namely 0.5 nm), and it has a very high temporal coherence with an energy spread of 0.5−0.7 eV. This provides the best conditions to extract the local chemical composition and spatial distribution of individual nanostructures by spectrum imaging (or spectrum line) mode. This mode consists of the acquisition of one EEL spectrum for each position of the probe scanning over a 2D (or 1D for spectrum-line mode) region of the sample.[53−56] Thus, it is possible to obtain not only the data to be analyzed but also the spatial statistics of a collection of spectra to be exploited.

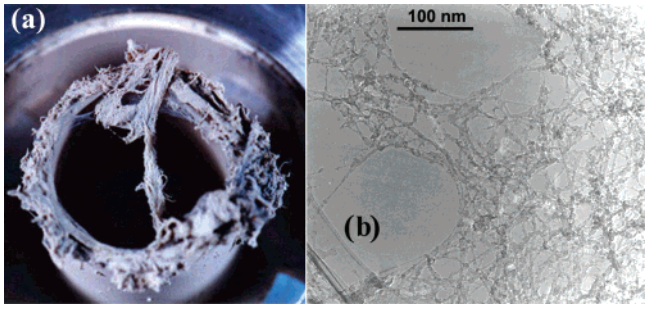

Figure 1. (a) Image of the as-synthesized product containing a high quantity of single-walled boron nitride nanotubes (SW-BNNTs). The web-like material displaying the filament aspect associated with the presence of BNNTs. (b) Low-magnification transmission electron microscopy (TEM) image showing the mixture of BNNTs and nanoparticles.

3. Results and Discussion

The reaction products collected on the filter and in a trap located in the outlet of the reactor chamber are displayed in Figure 1a. The soot sample has a filament/web aspect and shows a gray to light-beige color. These products consist of an inhomogeneous mixture of nanotubes and nanoparticles, Figure 1b. We have also found some large h-BN platelets (up to several microns in some cases) that are fragments of the target expelled by the laser.

Eighty percent of the nanotubes are single walled, other tubes being multi-walled with very few number of layers (primarily double-wall). The tubes are either isolated or organized in small bundles (2−10 tubes), as shown in Figure 2. The tube length is typically several hundreds of nanometers with a few tubes exceeding 1 μm. Their average diameter is close to 2 nm. HRTEM images reveal a clear tendency of these tubes to the zigzag configuration.[30] This preference has been recently confirmed by a statistical analysis of electron diffraction patterns recorded on more than 100 individual tubes where about 30% of the tubes were found to have an helicity of less than 5°.[57,58]

Spatially resolved EELS show that the BN structure of the tubes is sp^2 bonded with a boron to nitrogen ratio equal to unity.[44] Some of the tubes are partially filled, as we can see in the HRTEM image, Figure 3a. Figure 3b shows the spectrum line acquired across the filled nanotube. From the fine structures of the C−K edge of one of the spectra extracted from the

(49) Foutel-Richard, A. Ph.D. Thesis, Conservatoire National des Arts et Metiers, Paris, 2003.
(50) Dorval, N.; Foutel-Richard, A.; Cau, M.; Loiseau, A.; Attal-Trétout, B.; Cochon, J. L.; Pigache, D.; Bouchardy, P.; Krüger, V.; Geigle, K. P. *J. Nanosci. Nanotechnol.* **2004**, *4*, 450.
(51) Cau, M.; Dorval, N.; Cao, B.; Attal-Trétout, B.; Cochon, J. L.; Loiseau, A.; Farhat, S.; Scott, C. D. *J. Nanosci. Nanotechnol.* **2006**, *6*, 1.
(52) Arenal, R.; Stephan, O.; Kociak, M.; Taverna, D.; Colliex, C.; Rubio, A.; Loiseau, A. *AIP Conf.* **2004**, *723*, 293.
(53) Jeanguillaume, C.; Colliex, C. *Ultramicroscopy* **1989**, *28*, 252.
(54) Colliex, C.; Tence, M.; Lefevre, M.; Mory, C.; Gu, H.; Bouchet, D.; Jeanguillaume, C. *Mikrochim. Acta* **1994**, *71*, 114.
(55) Stephan, O.; Vlandas, A.; Arenal de la Concha, R.; Trasobares, S.; Loiseau, A.; Colliex, C. EMAG-03, *Institute of Physics Conference Series* **2004**, *179*, 437.
(56) Arenal, R.; Stephan, O.; Loiseau, A.; Colliex, C. *Microsc. Microanal.* **2007**, *13*, 1240.
(57) Arenal, R.; Kociak, M.; Loiseau, A.; Miller, D. *J. Appl. Phys. Lett.* **2006**, *89*, 073104.
(58) Arenal, R.; Kociak, M.; Loiseau, A.; Miller, D. J. *Microsc. Microanal.* **2006**, *12*, 578.

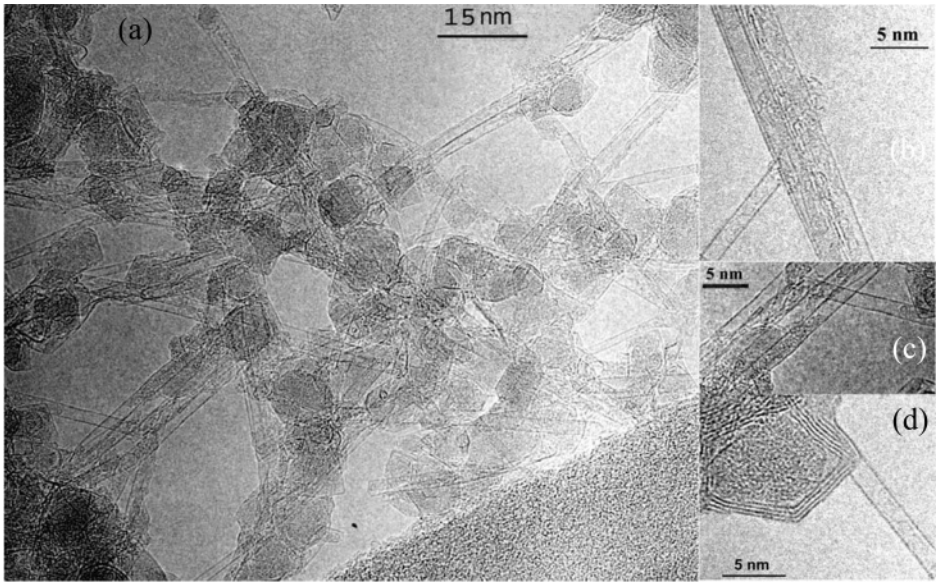

Figure 2. (a−d) High-resolution TEM (HRTEM) images of the different objects present in the samples: BNNTs (single-walled (individuals or organized in small bundles) and multi-walled (mostly double-walled)), cages, and other kinds of nanoparticles.

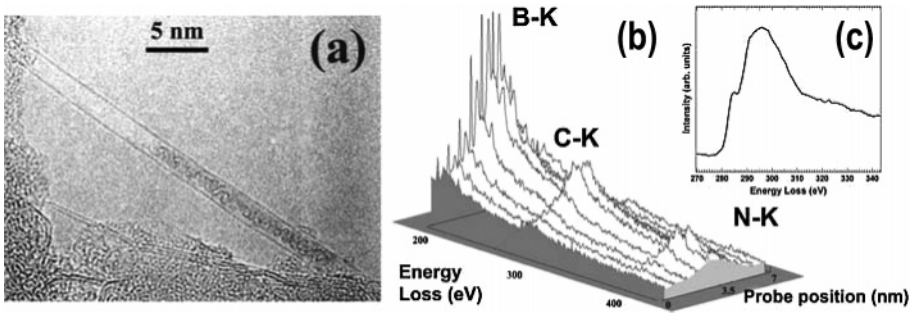

Figure 3. (a) HRTEM image showing a BNNT partially filled. (b) Electron energy loss (EEL) spectrum line across a NT partially filled. The K edges of boron (∼189 eV), carbon (∼284 eV), and nitrogen (∼399 eV) can be seen in these spectra. Boron and nitrogen forming the BN frame of the tube and uniformly distributed and the carbon inside the tube and not in substitution with the boron or nitrogen atoms of the BN network. (c) EEL spectrum showing the fine structures of the K edge of carbon, extracted from one of the spectra of the spectrum imaging (Figure 3b). Thus, from the analysis of the fine structures of this K-edge, we deduce that the carbon contained in the tubes corresponds to amorphous carbon.

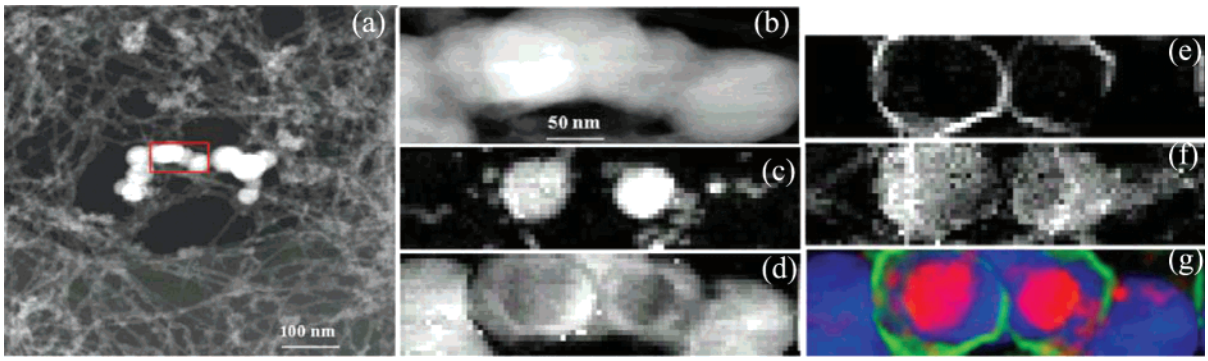

Figure 4. (a−b) High angular dark field (HADF) scanning TEM (STEM) images of a set of cages. (c−f) NNLS maps of boron, boron oxide, and boron nitride for the two extreme orientations (electron beam perpendicular and parallel to the **c** axis), respectively. (g) Superimposed spatial distributions of boron in its different chemical bonding states (RGB image obtained from the NNLS maps (Figure 4c−e): pure boron (red), boron nitride (green), and boron oxide (blue).

spectrum line (Figure 3c) we can deduce that this carbon corresponds to amorphous carbon. As suggested by the HRTEM image of Figure 3a, this is consistent with an amorphous carbon filling of the BN tube and this excludes the possibility of C atoms substitution within the BN network. The carbon content (in wt %) in the raw product was measured by means of an oxidant fusion method and infrared quantification. The result of these analyses was that the as-synthesized products only contain 0.03% of carbon. Carbon is also present inside some of the cages; see below (Figure 5a and b). After checking all the possible sources of this carbon contamination (hydrocarbons from the vacuum pump oil or from gas conductions, o-rings,...), we found that this weak quantity of carbon came from the target itself. The mechanism of filling will be explained below. We note that work is in progress to manufacture very pure h-BN targets and to eliminate this source of contamination.

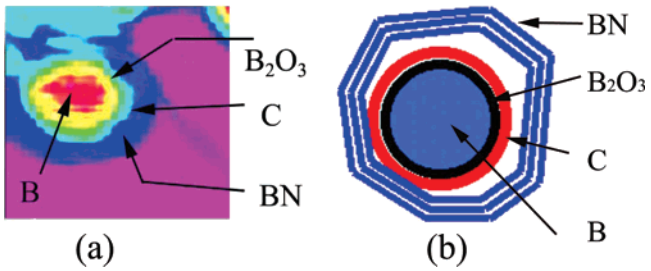

Figure 5. (a) Spatial distribution of the different materials of the complex cage extracted from a spectrum image recorded on one of those: boron core particle, covered by a film of boron oxide, surrounded by a film of amorphous carbon, and finally wrapping by boron nitride. The spatial distribution of the different materials is schematized in (b).

The size, shape, and structure of nanoparticles are very heterogeneous. They can be either attached at the nanotube tips, isolated, or encapsulated in BN shells (known as "cages" or "nanococoons"). We paid particular attention to the analysis of these nanoparticles as they are intimately involved in the formation mechanism of both tubes and cages. This analysis has been done by combining HRTEM and EELS techniques. In particular, we have employed a non-negative least-square (NNLS) fitting method to analyze the EELS spectrum-imaging recorded on the objects. This fitting method provides not only the chemical identification of the present elements but also the chemical bonding state of boron for the different existing compounds in these nano-objects via the analysis of the fine structures near the B−K absorption edge. This method is described more extensively in refs 44 and 56. In brief, it consists in the reconstruction of the experimental EEL spectrum from a linear combination of reference spectra of the different compounds. Chemical bonding maps at the nanometer scale can be extracted from the weights determined for the references.[44,56] In our case, these references were pure boron, boron oxide, and h-BN. Because h-BN is an anisotropic material, the fine structure of the B−K and N−K edges depend strongly on the orientation of momentum transfer (q) with respect to the lattice.[56,59,60] Thus, we obtained the NNLS maps of the h-BN of the two extrem orientations (the electron beam parallel and perpendicular to the anisotropic axis (**c**)), see Figure 4e and f and Figure 6d and e.

The encaged particles are nearly spherical in shape whereas the h-BN shells wrapping them are slightly polygonized, as attested by the examples shown in the HRTEM image Figure 2d. Figure 4a and b correspond to the high angular dark field (HADF) images of an assembly of these cages acquired simultaneously with the spectrum image. We employed the NNLS fitting method to obtain the complex composition of these cages. Figure 4c−f show the different NNLS maps corresponding to pure boron, boron oxide, and BN for the two extreme orientations of the electron beam with respect to the **c** axis. From these NNLS maps and their superimposition in Figure 4g (RGB image: red (boron), green (boron nitride), and blue (boron oxide)), we can deduce that the cages generally consist of a core pure boron particle covered by a thin layer of boron oxide and wrapped with h-BN shells. We also found that some of these nanococoons possess a layer of amorphous carbon between the layer of boron oxide and h-BN.[56] Figure 5a shows another example illustrating the spatial distribution of boron within a nanocage. Finally, a sketch showing the composition of the most complex situations of the cages is displayed in Figure 5b.

The knowledge of the composition and structure of the particles at the ends of the tubes is a key point for understanding the growth mechanism of the tubes. The size of these particles is only a few nanometers (≤10 nm). HRTEM observations indicate that the nanoparticles are most often encapsulated at the tip of the nanotubes (Figure 2). We have to notice that its diameter is systematically larger than that of the tube. Sometimes, a few tubes assembled into a bundle seem to emerge from the same particle. Such an example is analyzed in detail in Figure 6. The HRTEM image (Figure 6a) displays a nanoparticle at the end of a bundle of SW-BNNTs. The other end of the SW-BNNTs (isolated or organized in a bundle) shows an angular or a squared-off cap.[7,30,44] Nevertheless, due to the long length of the nanotubes, it is very difficult to obtain an image of both ends of one BNNT. This characteristic angular BN cap is due to the presence of squares instead of pentagons as in the case of CNTs.[7] It is also important to note that neither open-ended BNNTs nor amorphous caps were found in the samples.

We employed the NNLS method to analyze the EELS spectrum imaging acquired on this kind of object. Figure 6b−d shows the different NNLS maps for the present materials: pure boron and BN (the two extreme orientations of the electron beam against the **c** axis). The core particle is formed by pure boron, which is coated by the boron nitride network, forming the wall of the tube. In contrast with nanocages, it is worth mentioning that neither oxygen nor carbon were ever found in these particles.

We now discuss the formation mechanism of the tubes. The TEM results (HRTEM and EELS) strongly suggest that the formation of BNNTs originate in pure boron particles and that their growth proceeds by a root-based growth mechanism. Futhermore, the noncorrelation between the diameter of the particle and that of the tube argues for a growth perpendicular to the particle surface. We therefore have to account for the root growth from a boron particle and explain why the presence of oxygen in the boron particle leads to the formation of cage instead of a tube. The phenomenological model we propose here is based on three kinds of data: (i) the data on the synthesis parameters, (ii) the thermodynamic information provided by previous works on these systems (see Figure 7[61,62]), and (iii) the electron microscopy observations and analysis of our samples.

We argue that the formation of the SW-BNNTs takes place in a three-step process, as in a V-L-S model. The proposed model is sketched in Figure 8a. As indicated by the thermodynamic phase diagram of the B−N system (Figure 7a), upon heating by the laser beam, the h-BN compound of the target does not sublimate as graphite does but decomposes above 2600 K into gaseous nitrogen and in liquid boron. Boron gets then vaporized although the equilibrium vaporization temperature is far to be obtained at the surface of the target. The existence of the boron vapor state has recently been attested by in situ fluorescence measurements: the boron vapor has been detected

(59) Arenal, R.; Kociak, M.; Zaluzec, N. J. *Microsc. Microanal.* **2006**, *12*, 1188.
(60) Arenal, R.; Kociak, M.; Zaluzec, N. J. *Appl. Phys. Lett.* **2007**, *90*, 204105.
(61) Okamoto, K. *Phase Diagrams for binary alloys*; ASM International, U.S., 2000.
(62) Kasper, B. Ph.D. Thesis, Univeritat Stuttgart, 1996.

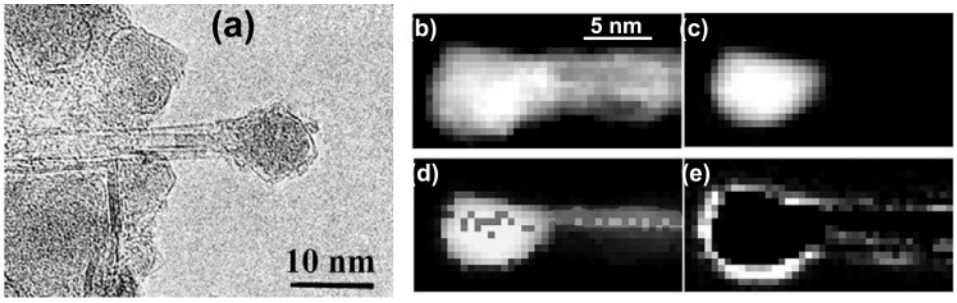

Figure 6. (a) HRTEM image of a particle at the end of a bundle of SW-BNNTs. (b) HADF image of a bundle composed by 2 SW-BNNTs. (c−e) NNLS maps of boron and boron nitride for the two extreme orientations (electron beam perpendicular and parallel to the **c** axis), respectively. It can clearly be seen that the core boron particle is surrounded by the boron nitride network.

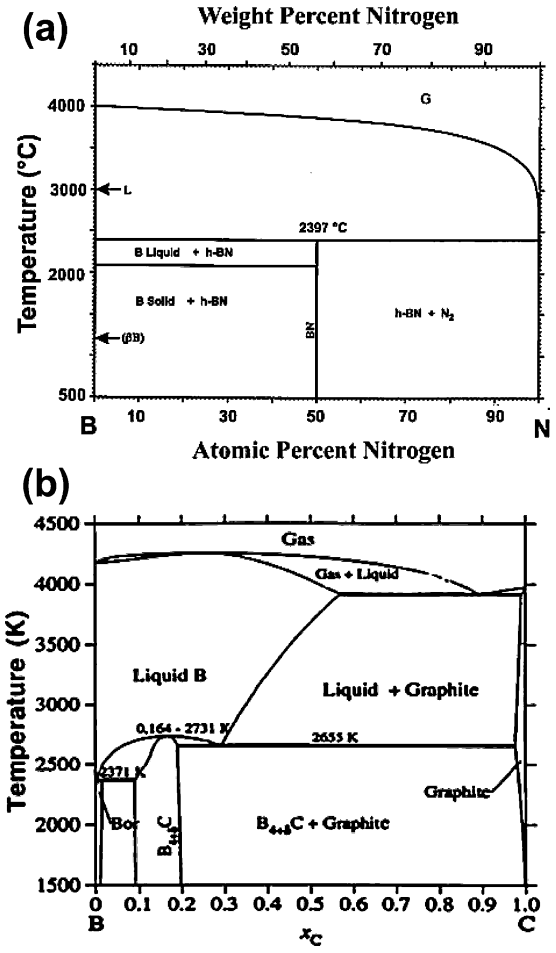

Figure 7. Phase diagram of the systems: (a) Boron and nitrogen (from ref 61), and (b) boron and carbon (from ref 62).

in a few millimeter thick layer just above the target surface.[63] The boron oxide binding is also decomposed and vaporized above 1800 °C. There are therefore two sources of boron available for the formation of the nanotubes. The efficiency of these two sources has been checked by replacing the h-BN material of the target by a boron oxide rod. BN nanotubes could be obtained with this alternative target but in lower yield compared to the h-BN target.

Upon cooling within the temperature gradient created by nitrogen flowing gas, the boron vapor condenses into small boron droplets. When the temperature falls below 2700 K

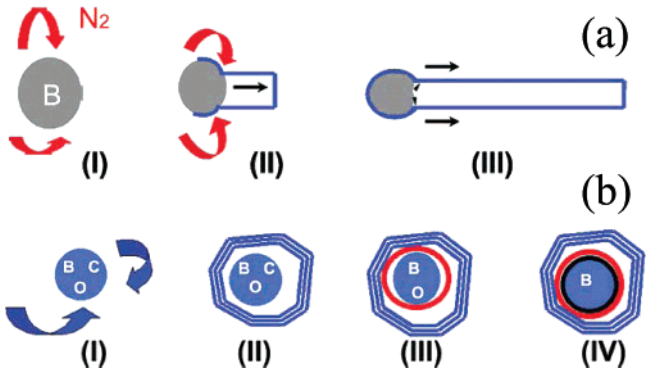

Figure 8. Sketches showing the phenomenological model for the formation of the tubes (a) and of the cages of BN (b). (a) Model is as follows: (a-i) formation of boron drops from the decomposition of h-BN and from the boron oxide of the target; (a-ii) reaction of these drops of boron with the nitrogen injected into the reaction chamber and with nitrogen coming from the h-BN target. Recombination of the boron and nitrogen to form boron nitride; (a-iii) incorporation of the nitrogen atoms at the root of the boron particle that achieves the growth of the tube. Concerning the cages and the presence of carbon and boron oxide filling these objects (for the carbon, it is also possible to find it inside of some of the BNNTs), the growth mechanism is: (b-i) and (b-ii) these steps correspond to the previous ones ((a-i) to (a-iii)), taking into account the dissolution of oxygen and carbon in the boron drops; (b-iii) and (b-iv) correspond to the segregation of the carbon and oxygen. For carbon, the segreagation occurs at temperature close to 2000 °C, whereas the segregation of the oxygen is at lower temperatures, toward 700 °C.

according to the B−N phase diagram, the boron droplets react with the nitrogen gas to form a sp^2 BN structure. In spite of the strong stability of the nitrogen molecule, the high reactivity of the liquid boron surface, at temperature as high as 2700 K, explains its ability to decompose this molecule. The nitrogen gas either comes from the carried gas or is issued from the decomposition of the target. This latter source has been checked by using argon as the carrier gas. As a consequence of the chemical reaction B−N_2, a sp^2 BN cap is formed at the surface of the particle (step I in Figure 8). It can progressively transform into a tube providing a continuous supply and decomposition of nitrogen at the surface of the particle (step II in Figure 8). This implies the initial size of the BN cap to be smaller than that of the particle to ensure a free surface access to the nitrogen gas. The nucleation process implies a root growth mechanism where nitrogen and boron atoms are incorporated in the BN network at the foot of the nanotube via its interface with the particle surface where the bonds are the most active. In this mechanism, the boron particle has a double role of growth support and of reactant.

This growth remains active as long as the boron particle is liquid, that is as long as the temperature is above 2300 K,

(63) Cau, M.; Dorval, N.; Attal-Trétout, B.; Cochon, J. L.; Cao, B.; Bresson, L.; Jaffrennou, P.; Silly, M.; Loiseau, A. *J. Nanosci. Nanotechnol.* **2007**, in press.

according to the B−N phase diagram (step III in Figure 8). Referring to the CARS measurements of temperature gradient of the nitrogen gas described above,[49−51,63] the solidification of the boron particle arises in a zone of the reactor chamber where the cooling rate is between 100 and 200 K/ms. This means that the growth of the tubes is abruptly stopped and explains the relative short length of SW-BNNTs compared to their carbon analogs synthesized via a continuous CO_2 laser vaporization of a NiCo-graphite target.[48] In that case indeed, growth occurs at lower temperature, that is, in a zone of the reactor where the cooling rate vanishes. In this zone, the temperature remains roughly constant and the residence time is a few tens of milliseconds, creating the conditions of a stationary regime suited for the growth of long tubes.[51] Finally, when the boron solidification occurs, the nitrogen atoms remaining at the surface of the particle react with surface boron atoms to build a BN sheet encapsulating the B particle.

It is a matter of fact that all boron particles do not give rise to nanotubes. First, certain particles can solidify prematurely without reacting with nitrogen. After opening the reactor, their contact with air leads to their transformation in boric acid. This explains the large quantity of boric acid found in the soot as detailed in ref 45. Second, the systematic presence of oxygen in the particles encaged in BN shells correlated with its systematic absence in particles at the tip of the tubes strongly suggests that oxygen inhibits the reaction between B and nitrogen and acts as a poison for the decomposition of the nitrogen molecule at the surface of boron particle. This effect has been checked replacing the h-BN target by a boron oxide rod. The additional oxygen in the reactor results in a drastic decrease in the nanotube yield.

The arguments put forward in the phenomenological model proposed here also account for the contamination of BN tubes by carbon and for the complex structure of BN cages. Both phenomena originate in the huge reactivity of liquid boron and its high ability to dissolve carbon and oxygen. In the case of carbon, the C−B phase diagram shown in Figure 7 attests the solubility of carbon to be larger than 30% at a temperature close to 2700 K. This solubility dramatically decreases as the temperature decreases and almost vanishes in solid boron. As a consequence, even if carbon is present with a very few concentration in the reactor, liquid boron droplets can absorb it. Carbon remains dissolved as long as boron particles remain liquid that is during the nanotube growth. Its incorporation in the BN network of the tube is very unlikely knowing that C−B and C−N bonds are much less stable than C−C and BN bonds.[64] Once the particle is solidified, carbon becomes insoluble and segregates by diffusing and precipitating at the surface of the particle. Because the particle is encapsulated by a BN sheet, the segregating carbon fills the cavity of the tube, thus explaining the presence of carbon in some tubes. O−B phase diagram displays the same properties as the C−B system except in the case of oxygen; its segregation from boron occurs at much lower temperature (1000 K). This difference in the segregation temperature of C and O explains the complex structure of the particles encaged in BN shells. As said above, the formation of the cages is indeed related to the presence of oxygen in the boron particle. The formation scenario is sketched in Figure 8b. During the formation of BN shells, C and O are dissolved into the particle (steps I and II). Once the particle is solidified, upon cooling, carbon segregates first (step III) followed by oxygen (step IV). This sequence accounts for the layered structure of the particle with, from outside to inside, the sheets of h-BN, a film of carbon, a film of boron oxide, and finally the core of pure boron.

(64) Nozaki, H.; Itoh, S. *J. Phys. Chem. Solids* **1996**, *57*, 41.

4. Conclusions

In summary, we have reported a detailed study of the samples containing a high quantity of single-walled boron nitride nanotubes, produced by a laser vaporization technique. From the data collected during the synthesis, those obtained from phase diagrams and those extracted from electron microscopy analyses (EELS at the nanometric scale and HRTEM), we proposed a phenomenological growth mechanism of the BNNTs. Our observations strongly support a root growth mechanism that involves three steps: (1) The decomposition by the laser of the boron oxide contained in the binder of the target as well as the h-BN crystallites of the target into nitrogen gas and liquid boron which gets finally vaporized in both cases. (2) Upon cooling, boron vapor condenses into small boron liquid droplets, which react with nitrogen gas, either coming from the carried gas or issued from the decomposition of the target, to form BN caps at the surface of the droplets. (3) Growth of the nanotubes results from the progressive incorporation of nitrogen and boron at the interface between the cap and the particle. The growth stops at the solidification of this boron core particle. We have also shown that the high reactivity of liquid boron is a source of different kinds of contamination. Contamination by carbon traces can lead to a partial filling of the tubes by an amorphous carbon material. Contamination by oxygen is found to inhibit the reaction $B-N_2$ and restrict the formation of a BN network to shells encapsulating the boron particle. The present analysis clarifies the properties governing the formation of SW−BNNT using a laser vaporization technique. One can in turn use these properties to adjust the synthesis conditions to improve the length and yield of the nanotubes. The presence of byproducts is indeed highly detrimental to the study of the nanotubes properties. It would be, for instance, desirable to increase the period of time where boron and nitrogen react with each other to form the tubes and to act on the temperature gradient to delay the solidification of the particle and to avoid any oxygen trace in the reactor. These are some avenues worth exploring in our future work.

Acknowledgment. This work was supported by the European Community research and training network COMELCAN (HPRN-CT-2000-00128). This work has been done within the framework of the GDRE "NanoE" (No. 2756) of the CNRS. We acknowledge helpful discussions with D. Pigache, N. Dorval, L. Bresson, A. Maguer, and A. Kanaev.

JA076135N